EPJ manuscript No.
(will be inserted by the editor)

Stretching dynamics of semiflexible polymers

B. Obermayer[1a], O. Hallatschek[2], E. Frey[1], and K. Kroy[3]
[1] Arnold Sommerfeld Center and Center for NanoScience, LMU München, Theresienstr. 37, 80333 München, Germany
[2] Lyman Laboratory of Physics, Harvard University, Cambridge, MA 02138, USA
[3] Institut für Theoretische Physik, Universität Leipzig Postfach 100920, 04009 Leipzig, Germany

the date of receipt and acceptance should be inserted later

Abstract. We analyze the nonequilibrium dynamics of single inextensible semiflexible biopolymers as stretching forces are applied at the ends. Based on different (contradicting) heuristic arguments, various scaling laws have been proposed for the propagation speed of the backbone tension which is induced in response to stretching. Here, we employ a newly developed unified theory to systematically substantiate, restrict, and extend these approaches. Introducing the practically relevant scenario of a chain equilibrated under some prestretching force $f_{\rm pre}$ that is suddenly exposed to a different external force $f_{\rm ext}$ at the ends, we give a concise physical explanation of the underlying relaxation processes by means of an intuitive blob picture. We discuss the corresponding intermediate asymptotics, derive results for experimentally relevant observables, and support our conclusions by numerical solutions of the coarse-grained equations of motion for the tension.

PACS. 61.41.+e Polymers, elastomers, and plastics – 87.15.La Biological and medical physics. Mechanical properties – 87.15.He Dynamics and conformational changes

The multifaceted viscoelastic properties of complex cellular structures such as the cytoskeleton have been intensively studied on very different levels of complexity [1]. Concerning their nature as networks of semiflexible polymers, it has recently become apparent that *prestressed* networks provide a realistic model for the mechanical properties of living cells [2]. Also, it has been found that the *dynamics* of semiflexible polymers and their networks is quite drastically altered by prestress [3–5]. On the level of single molecules, the scenario of a single semiflexible chain prestretched with a force $f_{\rm pre}$ that is suddenly exposed to a different stretching force $f_{\rm ext}$ at the ends may serve to explain quite generically the influence of prestress on single-polymer stretching and relaxation dynamics. Since the first force-extension measurements on DNA, which established the wormlike chain (WLC) model as a very good theoretical description for semiflexible polymers [6], technological advances towards significantly improved time- and force-resolution [7, 8] have made measurements on such more involved experimental setups possible. Theoretically, there exists a number of different approaches to the nonequilibrium dynamics of inextensible WLCs [9–12], most of them based on the concept of backbone tension, which is the force "holding the monomers together". Its key importance to the longitudinal dynamics has been recognized some time ago [13], but so far its influence has mainly been treated on the level of heuristic scaling arguments [13–16]. While such reasoning based on the WLC model has been used to analyze DNA relaxation experiments [17,18], a systematic theoretical description of propagation and relaxation of backbone tension has only recently been developed [19].

In the following, we consider an inextensible weakly-bending WLC in a simple solvent that is equilibrated under some tension $f_{\rm pre}$. At time $t = 0$, the chain is suddenly exposed to an external stretching force $f_{\rm ext}$ applied at its ends, the more interesting case being $f_{\rm ext} > f_{\rm pre}$. Our objective is to identify the dominant processes involved in the subsequent nonequilibrium dynamics, and, specifically, to determine how fast the contour stretches. The inextensibility prevents any contour stretching in the bulk unless the end regions have been pulled apart, which is however limited by longitudinal Stokes friction. The conclusion is that initially the external stretching force penetrates the contour only within a boundary layer of size $\ell_\parallel(t)$, see fig. 1. This comprises the relevant short-time effect and motivates the analysis presented in the remainder of the paper. After introducing model and equations of motion in sec. 1, we discuss in sec. 2 the stretching dynamics qualitatively by means of an intuitive "blob" picture inspired by the analogon for flexible polymers [20]. Hereby we regard only the special case $f_{\rm ext} \gg f_{\rm pre}$ since it captures all prominent features of the stretching dynamics. We obtain crossover scaling laws for $\ell_\parallel(t)$ that are compared to literature results [13–16]. In sec. 3, we explicitly calculate tension profiles by solving the equations of motion for the asymptotic regimes of sec. 2, and point out some inconsistencies of previous approaches [13, 16]. In the following

[a] e-mail: obermayer@physik.lmu.de

sec. 4 we present an algorithm to solve the equations of motion for the tension in intermediate and non-asymptotic regimes. Analytical and numerical results for experimentally relevant observables such as the change in the polymer's projected length are presented in the final sec. 5, where also some experimental implications are shortly discussed. A more systematic derivation of the asymptotic equations of motion and their solutions, as well as details of the numerical approach are shifted to the appendices.

1 Equations of motion

Conformations of wormlike chains are described as continuous space curves $\boldsymbol{r}(s,t)$ of total contour length L. In the WLC-Hamiltonian [21], bending energy is proportional to the square of the local curvature.[1] We set the proportionality constant (the bending rigidity) $\kappa \equiv 1$. Below, we will also set the friction coefficient (per length) ζ to unity. In these units, tension is a length^{-2} and time a length^4. The persistence length of a free WLC in equilibrium is then given by $\ell_\mathrm{p} = (k_\mathrm{B}T)^{-1}$. We account for the local inextensibility $|\boldsymbol{r}'| \equiv |\partial_s \boldsymbol{r}| = 1$ by introducing the backbone tension $f(s,t)$ as a Lagrange multiplier function [9]. In the limit of small transverse displacements $\boldsymbol{r}_\perp$ from a straight line, the corresponding *weakly-bending* Hamiltonian reads

$$\mathcal{H} = \frac{1}{2}\int_0^L \mathrm{d}s[\boldsymbol{r}_\perp''^2 + f\boldsymbol{r}_\perp'^2]. \tag{1}$$

Comparing contributions from bending $\boldsymbol{r}_\perp^2/l_\mathrm{b}^4$ and from tension $f\boldsymbol{r}_\perp^2/l_\mathrm{b}^2$ on the scaling level, we infer that on length scales smaller than the *blob size* $l_\mathrm{b} \equiv f^{-1/2}$ [24] (see fig. 1), the conformation is dominated by bending forces, and only on larger scales perturbed by the tension contributions. In equilibrium, each blob carries a stored length of $l_\mathrm{b}^2/\ell_\mathrm{p}$ [21], which is simply the thermal contraction compared to the straight conformation. The weakly-bending assumption requires $l_\mathrm{b} \ll \ell_\mathrm{p}$. This can be realized both for short stiff polymers ($L \ll \ell_\mathrm{p}$) and for strongly prestretched flexible WLCs ($f_\mathrm{pre} \gg \ell_\mathrm{p}^{-2}$).

The overdamped motion of the transverse displacements is described by the equation $\partial_t \boldsymbol{r}_\perp = -\delta\mathcal{H}/\delta\boldsymbol{r}_\perp + \boldsymbol{\xi}_\perp$, which captures the balance of viscous friction, bending and tension forces resulting from the energy [eq. (1)], and stochastic noise $\boldsymbol{\xi}_\perp$:

$$\partial_t \boldsymbol{r}_\perp = -\boldsymbol{r}_\perp'''' + (f\boldsymbol{r}_\perp')' + \boldsymbol{\xi}_\perp. \tag{2}$$

Introduced as Lagrange multiplier function, the tension $f(s,t)$ has to be computed through the inextensibility constraint, which makes eq. (2) highly nonlinear. In spite of that, it can be simplified quite significantly in the weakly-bending limit [19]: spatial variations in the tension f can be neglected. It turns thus into a linear equation that can be decomposed into normal modes,

$$\partial_t \boldsymbol{r}_\perp = -q^4\boldsymbol{r}_\perp - q^2 f\boldsymbol{r}_\perp + \boldsymbol{\xi}_\perp, \tag{3}$$

and solved using the response function

$$\chi_\perp(q;t,t') = \mathrm{e}^{-q^2[q^2(t-t') + \int_{t'}^t f\mathrm{d}\tilde{t}]}\Theta(t-t'). \tag{4}$$

Here, $\Theta(t)$ is the Heaviside function. This allows to evaluate a characteristic quantity of high relevance for our approach: the *stored length density* $\varrho \equiv \frac{1}{2}\langle \boldsymbol{r}_\perp'^2\rangle$ that measures the average amount of contour length stored in thermal undulations:

$$\varrho = \sum_q \left[\varrho_0(q)\chi_\perp^2(q;t,0) + \frac{2q^2}{L\ell_\mathrm{p}}\int_0^t \mathrm{d}t'\chi_\perp^2(q;t,t')\right], \tag{5}$$

by evaluating the noise correlation $\langle \boldsymbol{\xi}_{\perp,k}(t)\boldsymbol{\xi}_{\perp,q}(t')\rangle = 4/(L\ell_\mathrm{p})\delta_{k,q}\delta(t-t')$. The initial mode spectrum of a polymer equilibrated under the force f_pre follows via equipartition from the Hamiltonian [eq. (1)]:

$$\varrho_0(q) = \frac{1}{L\ell_\mathrm{p}(q^2 + f_\mathrm{pre})}. \tag{6}$$

However, as discussed in the introduction and illustrated in fig. 1, neither the tension f nor the stored length density ϱ are in fact spatially constant. Compared to the "fast" transverse undulations though, their spatial dependence is rather slow and can thus be re-introduced within an adiabatic approximation. This convenient practice is rigorously justified by means of a multiple scale analysis in ref. [25]. Its main result is that the curvature in the spatially slowly varying tension profile is given by changes in the stored length density $\varrho(s,t)$, which inherits its slow arclength dependence adiabatically from the tension $f(s,t)$ via eq. (4):

$$\partial_s^2 f(s,t) = -\partial_t \varrho(s,t). \tag{7}$$

Integrating eq. (7) over time yields

$$\partial_s^2 F(s,t) = -[\varrho(s,t) - \varrho(s,0)], \tag{8}$$

where we have introduced the integrated tension

$$F(s,t) \equiv \int_0^t \mathrm{d}t' f(s,t'). \tag{9}$$

Using eq. (5) with a spatial dependence of $\varrho(s,t)$ given through $f(s,t)$ in the exponent of $\chi_\perp(q;t,t')$, and taking the continuum limit $L \to \infty$, renders eq. (8) in the explicit form [25]

$$\partial_s^2 F(s,t) = \int_0^\infty \frac{\mathrm{d}q}{\pi\ell_\mathrm{p}}\left\{\frac{1 - \mathrm{e}^{-2q^2[q^2t + F(s,t)]}}{q^2 + f_\mathrm{pre}} - 2q^2\int_0^t \mathrm{d}t'\,\mathrm{e}^{-2q^2[q^2(t-t') + F(s,t) - F(s,t')]}\right\}. \tag{10}$$

Initial and boundary conditions for our setup are

$$F(s, t<0) = f_\mathrm{pre}t \quad \text{and } F(0,t) = F(L,t) = f_\mathrm{ext}t. \tag{11}$$

[1] Note that this harmonic dependence has lately been under some debate concerning DNA bending angle distributions on short length scales [22,23].

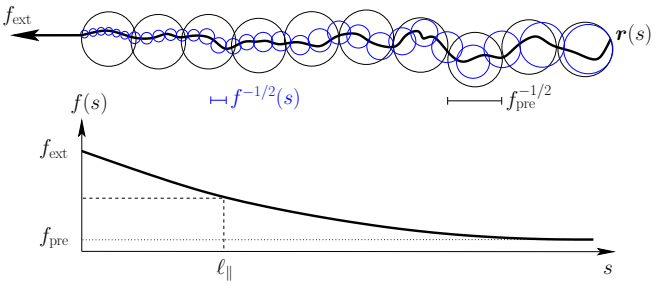

Fig. 1. Pulling a prestretched filament. Thermal fluctuations in the contour $\boldsymbol{r}(s)$ are straightened first in a boundary layer of width $\ell_\parallel(t)$. At any time t, blobs of size $f_{\rm pre}^{-1/2}$ and $f^{-1/2}(s)$ are associated with the prestretching force $f_{\rm pre}$ and the actual local backbone tension $f(s)$, respectively.

For a detailed derivation of eq. (10) we refer the interested reader to ref. [25]. Here we only comment on a few important points. First, a proper decomposition of eq. (2) into its eigenmodes depends on the choice of boundary conditions and yields, in general, eigenvalues different from the simple $q^2[q^2+f]$ used here. Second, we are going to extend eq. (10), which applies to the continuum limit $L\to\infty$, to "real" polymers of finite length. Both issues are resolved by recognizing that on short times the *relevant* modes have wavelength much shorter than L, that long wavelengths are initially suppressed by prestretching with $f_{\rm pre}$, and that therefore the influence of the boundary conditions and the discreteness of the mode spectrum is small. Below, we will discuss the relevance of these effects for pertinent observables. Finally, the underlying scale separation between small-scale "fast" transverse fluctuations and large-scale "slow" tension dynamics can be readily rationalized by observing that the tension varies only over distances on the order of $\ell_\parallel$, which is at any time much larger than the correlation length for transverse fluctuations [19]:

$$\ell_\perp(t)\simeq\begin{cases}t^{1/4}, & \text{for } t\ll f^{-2}\\ (f\,t)^{1/2}, & \text{for } t\gg f^{-2}\end{cases}\qquad(12)$$

Eq. (12) is easily understood as the expression of the dynamic force balance between transverse friction forces $r_\perp/t$ and bending $r_\perp/\ell_\perp^4$ or tension terms $fr_\perp/\ell_\perp^2$, respectively, i.e., by analyzing eq. (2) on a scaling level. It displays the crossover between "free" (bending-dominated) relaxation within blobs and "forced" (tension-driven) relaxation on larger scales.

2 Blob picture of stretching dynamics

A qualitative yet rather thorough understanding of the nonequilibrium stretching dynamics can be gained already from the special case $f_{\rm ext}\gg f_{\rm pre}$, i.e., for the scenario of a sudden strong increase in stretching force. It is useful to interpret the correlation length $\ell_\perp(t)$ of eq. (12) as an *equilibration length* for transverse fluctuations. At any time t, segments of length $\ell_\perp$ are in equilibrium with their surroundings [15,19]. Upon applying the external force $f_{\rm ext}$, the contour starts to stretch within a boundary layer of size $\ell_\parallel$. Decomposing the latter into $\ell_\parallel/\ell_\perp$ segments of length $\ell_\perp$, the extension δ of each segment in response to the local tension $f(s)$ can be estimated within equilibrium theory. At this point we use the blob picture: the prestretching force $f_{\rm pre}$ and the local tension $f(s)$, which builds up after the external force is applied, induce blobs at different length scales. Associated with the weaker prestretching force are large blobs of constant size $f_{\rm pre}^{-1/2}$, and the stronger local tension corresponds to small blobs of varying size $f^{-1/2}(s)$, respectively (see fig. 1). The extension δ depends on "how many" blobs are contained in a segment (or vice versa). Three cases can be distinguished for $f_{\rm ext}\gg f_{\rm pre}$:

- $\ell_\perp\ll f^{-1/2}(s)$: a large number of segments $\ell_\perp$ are in either type of blob; hence, bending forces dominate and the extension follows from linear response [26]: $\delta\simeq\ell_\perp^4 f(s)/\ell_{\rm p}$.
- $f^{-1/2}(s)\ll\ell_\perp\ll f_{\rm pre}^{-1/2}$: segments $\ell_\perp$ near the boundary are larger than the small blobs corresponding to the local tension. Hence, they get almost completely stretched, and essentially all initially stored length is pulled out. Being still smaller than the large blobs of size $f_{\rm pre}^{-1/2}$, these segments correspond to short stiff *initially unstretched* chains, thus their extension is $\delta\simeq\ell_\perp^2/\ell_{\rm p}$.
- $f_{\rm pre}^{-1/2}\ll\ell_\perp$: now the segments $\ell_\perp$ are larger than any of the blobs and release the stored length of a taut *string of blobs*. In a segment, there are $\ell_\perp/f_{\rm pre}^{-1/2}$ large blobs of size $f_{\rm pre}^{-1/2}$ each with stored length $1/(\ell_{\rm p}f_{\rm pre})$, hence $\delta\simeq\ell_\perp/(\ell_{\rm p}f_{\rm pre}^{1/2})$.

The above results for the extension δ and eq. (12) for the length $\ell_\perp$ of the segments can now be used to estimate the total stretching $(\ell_\parallel/\ell_\perp)\delta$ of the chain's boundary layer. On the scaling level, we can set $f(s)=f_{\rm ext}$ for the relevant segments near the boundary. The size $\ell_\parallel$ of the boundary layer is the central quantity still to be determined. According to its definition, it is obtained by requiring that the total longitudinal friction on the order of $\ell_\parallel(\ell_\parallel/\ell_\perp)\delta/t$ equals the driving force $f_{\rm ext}$, i.e., $\ell_\parallel(t)$ scales as

$$\ell_{\rm p}^{1/2}t^{1/8}, \qquad \text{for } t\ll f_{\rm ext}^{-2} \qquad(13a)$$
$$\ell_{\rm p}^{1/2}(f_{\rm ext}\,t)^{1/4}, \qquad \text{for } f_{\rm ext}^{-2}\ll t\ll(f_{\rm ext}f_{\rm pre})^{-1} \qquad(13b)$$
$$\ell_{\rm p}^{1/2}f_{\rm pre}^{1/4}(f_{\rm ext}\,t)^{1/2}, \qquad \text{for } (f_{\rm ext}f_{\rm pre})^{-1}\ll t. \qquad(13c)$$

The first case [eq. (13a)] has already been derived by Everaers et al. [15] (EJAM) based on a similar argument. This universal initial regime also shows up for other force protocols [19,27], including the case where $f_{\rm ext}<f_{\rm pre}$. The second scaling law [eq. (13b)] has first been proposed by Seifert, Wintz, and Nelson [13] (SWN). This intermediate regime emerges if the large and small blobs have very different size, i.e., either for vanishing prestretching

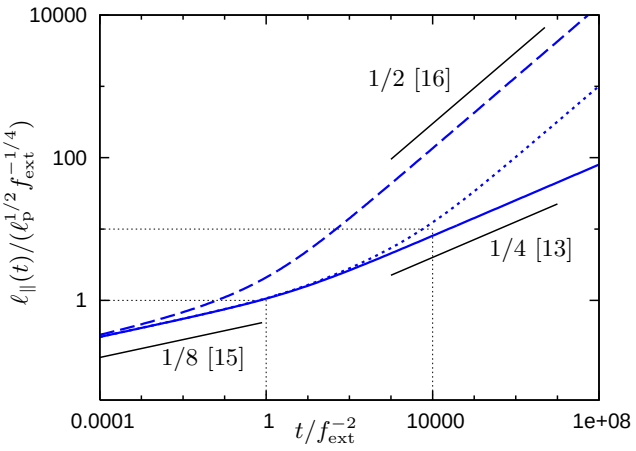

Fig. 2. Scaling of the boundary layer size $\ell_\parallel(t)$ (log-log scale) for different force ratios $f_{pre}/f_{ext} = 1/2$ (long-dashed), $f_{pre}/f_{ext} = 10^{-4}$ (short-dashed), and $f_{pre} = 0$ (solid). $\ell_\parallel$ is extracted from numerical solutions of eq. (10). The asymptotic scaling laws of eq. (13) are indicated by dark lines.

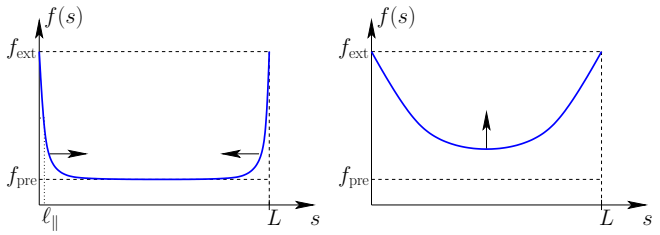

Fig. 3. Schematic tension profiles for $f_{ext} > f_{pre}$. Left: propagation regime $t \ll t_L^\parallel$. Near the ends, the tension falls off over the distance $\ell_\parallel \ll L$ and is constant in the bulk. Right: relaxation regime $t \gg t_L^\parallel$. The tension relaxes towards its final equilibrium value $f \equiv f_{ext}$. For times $t \gg t_\star$ the difference between f and f_{ext} is small.

force or for strong force scale separation $f_{ext} \gg f_{pre}$. However, *only near the boundary* the different blobs differ in size. Accordingly, the contour stretches significantly only where the actual tension is already strongly different from its bulk value f_{pre}. Thus, as pointed out in ref. [14], *tension propagates faster than stretching is achieved*. Finally, for long times $t \gg (f_{ext} f_{pre})^{-1}$, we get a result similar to the one by Brochard, Buguin, and de Gennes (BBG) derived in ref. [16], where they assumed the tension to be locally equilibrated. Note, however, that we obtain a more detailed force dependence in eq. (13c). In sec. 3 below, this discrepancy is traced back to a subtlety of the limit $f_{pre} \to 0$. Both results agree only for $f_{ext} \approx f_{pre}$.

In the latter case, i.e., if the stretching force is changed only by a small amount $\Delta f \equiv f_{ext} - f_{pre} \ll f_{ext}$, the results for the segment extension δ are reduced by a factor $\Delta f/f_{ext}$. Because the different blobs have then essentially the same size, the force balance argument leading to eq. (13) (here with the driving force Δf) yields only two cases: $\ell_\parallel \simeq \ell_p^{1/2} t^{1/8}$ [15] for $t \ll f_{ext}^{-2}$ and $\ell_\parallel \simeq \ell_p^{1/2} f_{ext}^{3/4} t^{1/2}$ [16] for $t \gg f_{ext}^{-2}$. There is no intermediate $t^{1/4}$-regime.

Summarizing the preceding discussion, we found intermediate asymptotic scaling laws for the boundary layer size $\ell_\parallel(t)$ by estimating the stretching of segments $\ell_\perp$ within a blob picture and balancing the resulting longitudinal friction with the driving force. As a rule of thumb, the small blobs corresponding to the stronger force $f(s)$ decide whether a segment gets stretched "just a little" or "much", and the large blobs corresponding to the weaker force f_{pre} determine how much "much" actually is. To illustrate the power laws given in eq. (13), numerical results for $\ell_\parallel(t)$ are shown in fig. 2, where $\ell_\parallel(t)$ has been extracted from tension profiles computed by numerically solving eq. (10), see sec. 4. The intermediate asymptotic scaling is clearly visible for small and large times, and the $t^{1/4}$-regime of eq. (13b) appears for very strong force scale separation only. We proceed with a more detailed discussion based on tension profiles to elucidate the similarities and differences between our results and previous work.

3 Tension profiles

Instead of repeating the rigorous analysis of eq. (10) presented in ref. [27] and extending it to deal with two force scales, we will analyze three different asymptotes of eq. (10) motivated by physical considerations that lead to the quite different approximations employed previously [13, 15, 16]. As in sec. 2, we are primarily interested in the case $f_{ext} \gg f_{pre}$ and discuss other possibilities only incidentally. A more systematic and complete derivation is presented in appendix A.1. Having motivated these approximations and derived their asymptotic validity, we will find that the partial integro-differential equation (PIDE) [eq. (10)] reduces to simpler differential equations that can again be solved in two regimes (see fig. 3):

1. In the *propagation regime* $t \ll t_L^\parallel$ with $t_L^\parallel$ defined via $\ell_\parallel(t_L^\parallel) = L$, the tension profile falls off over the (increasing) distance $\ell_\parallel(t)$. Because then $\ell_\parallel(t) \ll L$, we may neglect the presence of a second end, set $L \to \infty$ and work with a so-called "semi-infinite" contour. For this regime we will show that, using SWN's and BBG's approaches, the resulting differential equations do not always lead to tension profiles with the required features (compare fig. 3), namely that $F(s)$ decays from $f_{ext}\, t$ (at the boundary) to $f_{pre}\, t$ (in the bulk) within a region of size $\ell_\parallel$, and that $F(s) \equiv f_{pre}\, t$ is flat in the bulk.
2. In the *relaxation regime* $t \gg t_L^\parallel$, the influence of the second end cannot be neglected. However, it turns out that for late times $t \gg t_\star$, the resulting tension profile can be obtained by expanding eq. (10) about the final equilibrium profile: $F(s,t) = f_{ext}\, t + \delta F(s,t)$. To lowest order, the correction δF is then a simple parabola with constant curvature given by the right hand side of eq. (10) evaluated with $F \equiv f_{ext}\, t$. The time $t_\star$ is the crossover time to a regime $t \gg t_\star$ where

$\delta F \ll f_{\rm ext}\, t$ is in fact small, and can therefore be defined via $\delta F(t_\star) \simeq f_{\rm ext} t_\star$. With one exception, we will find that $t_\star \simeq t_L^\parallel$. Some of the relaxation regimes have already been discussed in refs. [19,27] for related force protocols. We shift their analysis to appendix A.2 and consider in the following only generically new results.

The scaling of the crossover times $t_L^\parallel$ and $t_\star$ between the respective propagation and relaxation regimes will be derived along the way and is summarized in table 1 below. It is different for the three approximations analyzed in the remainder of this section and depends on the magnitude of $f_{\rm pre}$ and $f_{\rm ext}$ relative to the critical force $f_{\rm c} = \ell_{\rm p}^2/L^4$. Similar to the well-known Euler buckling force $f^* \propto L^{-2}$ that represents a critical threshold above which forces significantly disturb the *transverse* dynamics [3,19], the force $f_{\rm c}$ can be seen as threshold force for the *longitudinal* dynamics.

3.1 Linear approximation

The two limits discussed above arise quite naturally within the *linear approximation* to eq. (10), which is similar to the approach by EJAM [15]. It consists in treating the prestretching force $f_{\rm pre}$ as well as the tension F as small perturbations with respect to the dynamically relevant bending contributions. From eq. (12) and its interpretation we infer that this approximation is justified in the limit $t \ll f^{-2}$. Because the tension f varies between $f_{\rm ext}$ at the boundary and $f_{\rm pre}$ in the bulk, this certainly holds if $t \ll \min(f_{\rm ext}^{-2}, f_{\rm pre}^{-2})$. In this case, we approximate the response function [eq. (4)] by $\chi_\perp(q;t,t') \approx \mathrm{e}^{-2q^4 t}(1-2q^2F)$ and the initial mode spectrum [eq. (6)] by $(q^2+f_{\rm pre})^{-1} \approx q^{-2}(1-f_{\rm pre}/q^2)$, and obtain eq. (10) to linear order in F and $f_{\rm pre}$ as:

$$\partial_s^2 F(s,t) \approx \int_0^\infty \frac{\mathrm{d}q}{\pi\ell_{\rm p}} \Bigg[-\frac{f_{\rm pre}}{q^4}\left(1-\mathrm{e}^{-2q^4 t}\right) + 2F(s,t) - 4q^4 \int_0^t \mathrm{d}t'\, F(s,t')\mathrm{e}^{-2q^4(t-t')} \Bigg]. \quad (14)$$

Using the Laplace transform $\tilde F(s,z) = \mathcal{L}\{F(s,t)\}$, this reads

$$\partial_s^2 \tilde F(s,z) = \int_0^\infty \frac{\mathrm{d}q}{\pi\ell_{\rm p}} \left[-\frac{2f_{\rm pre}}{z(z+2q^4)} + \tilde F(s,z)\frac{2z}{z+2q^4} \right], \quad (15)$$

which, after performing the q-integral, reduces to:

$$\lambda^2\, \partial_s^2 \tilde F = \tilde F - \frac{f_{\rm pre}}{z^2}. \quad (16)$$

Here, $\lambda(z) = 2^{3/8}\ell_{\rm p}^{1/2} z^{-1/8}$ is a dynamic length scale denoting the size of spatial variations in $\tilde F(s,z)$. It is therefore directly related to $\ell_\parallel(t)$. With the boundary conditions $\tilde F(0,z) = \tilde F(L,z) = f_{\rm ext}/z^2$, the solution to eq. (16) reads

$$\tilde F(s,z) = \frac{\Delta f}{z^2}\frac{\cosh[(L-2s)/2\lambda]}{\cosh(L/2\lambda)} + \frac{f_{\rm pre}}{z^2}, \quad (17)$$

where $\Delta f \equiv f_{\rm ext} - f_{\rm pre}$ is the force difference.

If $L \gg \lambda$, the tension profile eq. (17) varies only close to the boundaries, as it is characteristic for the propagation regime. Near $s = 0$, it simplifies to

$$\tilde F(s,z) \approx \frac{\Delta f}{z^2}\mathrm{e}^{-s/\lambda} + \frac{f_{\rm pre}}{z^2}, \quad (18)$$

which can be backtransformed [27] to

$$F(s,t) = \Delta f\, t\, \phi(s/\ell_\parallel(t)) + f_{\rm pre} t, \quad (19)$$

where $\phi(\xi) \approx \exp[-2^{-3/8}\xi/\Gamma(15/8)]$ is a scaling function that depends only on the ratio $\xi = s/\ell_\parallel(t)$ with a boundary layer size $\ell_\parallel(t) = \ell_{\rm p}^{1/2} t^{1/8}$ that scales as predicted in eq. (13a). The requirement $L \gg \lambda$ translates into $t \ll t_L^\parallel$ with $t_L^\parallel \simeq L^8/\ell_{\rm p}^4$.

The relaxation regime corresponds to the complementary limit $L \ll \lambda$, or equivalently $t \gg t_L^\parallel$. Here we find, as anticipated, that the tension $F(s,t)$ differs for $t \gg t_\star$ from the flat profile $f_{\rm ext}\, t$ only by a subdominant term $\delta F \simeq f_{\rm ext} t^{3/4} L^2/\ell_{\rm p}$ with a (trivial) parabolic s-dependence. By evaluating $\delta F(t_\star) = f_{\rm ext} t_\star$ we find $t_\star \simeq L^8/\ell_{\rm p}^4 \simeq t_L^\parallel$. See appendix A.2 for details.

3.2 Taut-string approximation

In this approximation introduced by SWN [13], bending and thermal forces are neglected after the preparation of an initial equilibrium configuration. As discussed below eq. (12), bending contributions are locally negligible against tension in the long-time limit $t \gg f^{-2}$. The transverse displacement modes effectively obey $\partial_t \boldsymbol{r}_\perp = -q^2 f \boldsymbol{r}_\perp$, see eq. (3). The stored length density relaxes as $\varrho = \sum_q \varrho_0(q)\exp[-2q^2F]$, and eq. (7) reads [27]:

$$\partial_s^2 F = \int_0^\infty \frac{\mathrm{d}q}{\pi\ell_{\rm p}} \frac{1-\mathrm{e}^{-2q^2F}}{q^2+f_{\rm pre}}. \quad (20)$$

Depending on the magnitude of the product $f_{\rm pre}F$ (which is dimensionless in our units), this has two asymptotes:

$$\partial_s^2 F \sim \begin{cases} \sqrt{2F/\pi\ell_{\rm p}^2}, & \text{if } f_{\rm pre}F \ll 1, \quad (21a) \\ 1/(2f_{\rm pre}^{1/2}\ell_{\rm p}), & \text{if } f_{\rm pre}F \gg 1. \quad (21b) \end{cases}$$

These will be discussed only for the propagation regime.

Estimating $F \simeq f_{\rm ext} t$ near the boundary, the first asymptotics is realized for intermediate times $f_{\rm ext}^{-2} \ll t \ll (f_{\rm pre} f_{\rm ext})^{-1}$. The differential equation (21a) is solved [27] by the scaling ansatz $F(s,t) \equiv f_{\rm ext} t\, \phi(s/\ell_\parallel(t))$, with the boundary layer size $\ell_\parallel(t) = \ell_{\rm p}^{1/2}(f_{\rm ext}\, t)^{1/4}$ as in eq. (13b), which implies $t_L^\parallel \simeq L^4/(\ell_{\rm p}^2 f_{\rm ext})$. This scaling ansatz gives

a tension that decays within a length $\ell_\parallel(t)$ as expected, but does it meet our expectations in the bulk? If $f_{\rm pre} = 0$, corresponding to the "pulling"-scenario of ref. [19], the scaling form $F = f_{\rm ext} t\, \phi(\xi)$ with $\xi = s/\ell_\parallel(t)$ can smoothly be extended to the bulk tension, which obeys $F \equiv \partial_s^2 F \equiv 0$ [27]:

$$\phi(\xi) = \left[1 - \frac{\xi}{(72\pi)^{1/4}}\right]^4 \Theta\left((72\pi)^{1/4} - \xi\right). \qquad (22)$$

If $f_{\rm pre}$ is finite, however, the bulk tension has nonzero magnitude and eq. (21) would yield nonzero curvature for the expectedly flat bulk profile. Hence, for finite $f_{\rm pre}$ the taut-string approximation is not valid along the whole contour, but only in a finite region near the boundary. *In this case it does not represent an intermediate asymptotic regime of eq.* (10).

The second asymptotics (21b), realized for late times $t \gg (f_{\rm pre} f_{\rm ext})^{-1}$, implies zero curvature for the tension $f = \partial_t F$ everywhere. The relaxation changes its character: most of the initially excited modes have relaxed (the long-wavelength contributions have been "cut off" by the pre-stretching force from the beginning). This corresponds to an almost completely stretched contour under linearly decreasing tension in the boundary layer. However, eq. (21b) is not sufficient to describe the specific shape of the associated tension profiles which have to be constant in the bulk. One needs to include thermal noise.[2]

3.3 Quasi-static approximation

The preceding paragraph revealed a problem with the taut-string approximation for $f^2 t \gg 1$ and $f_{\rm pre} F \gg 1$: the right hand side of eq. (21b) becomes time-independent and the deterministic relaxation saturates, so that the subsequent dynamics is purely of stochastic origin. This allows to simplify it as a quasi-equilibrium process. Following the approach of BBG [16], one can assume the filament to be equilibrated under the local tension $f(s,t) = \partial_t F(s,t)$. From the continuum approximation to eq. (6), the stored length density is $\varrho = \int \frac{{\rm d}q}{\pi \ell_{\rm p}} (q^2 + \partial_t F)^{-1} = (\partial_t F)^{-1/2}/(2\ell_{\rm p})$. According to eq. (8), this adds a small but relevant contribution to eq. (21b) [27]:

$$\partial_s^2 F = \frac{1}{2\ell_{\rm p}} \left[f_{\rm pre}^{-1/2} - (\partial_t F)^{-1/2} \right]. \qquad (23)$$

By taking a time derivative we get

$$\partial_s^2 f = \frac{\partial_t f}{4 \ell_{\rm p} f^{3/2}}. \qquad (24)$$

We discuss the quasi-static approximation both for the propagation and the relaxation regime.

[2] SWN's "noiseless" simulations [13] for a prestretched chain yield the correct scaling $\ell_\parallel(t) \propto t^{1/2}$ and linear tension profiles, but (as their scaling argument indicates) a straight string drawn through a viscous solvent gives a linear profile, irrespective of thermal noise.

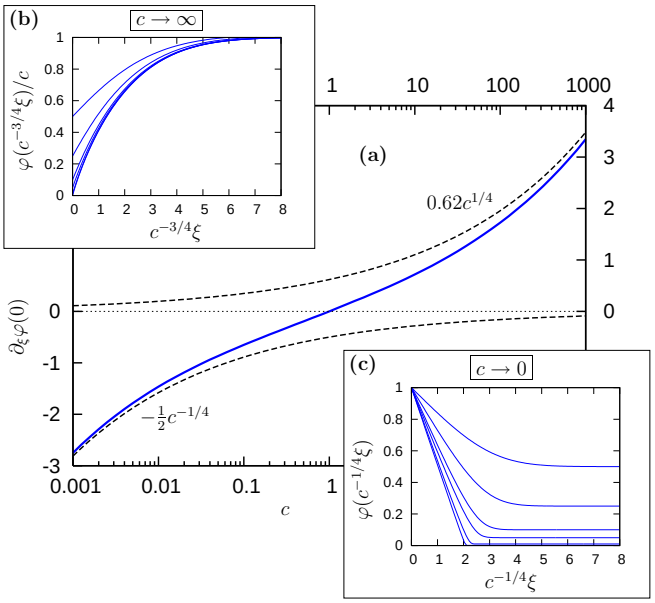

Fig. 4. Numerical solutions of eq. (25) for the scaling function $\varphi(\xi)$ of the tension profile $f(s,t)$. (a) Plot of the slope $\partial_\xi\varphi(0)$ at the boundary (solid line) vs. force ratio $c = f_{\rm pre}/f_{\rm ext}$ (log-scale) with analytical asymptotes for $c \to 0$ and $c \to \infty$, respectively (dashed lines). (b) The scaling functions ($c = 2, 4, 10, 20, 100, 1000$ from top to bottom) asymptotically collapse for $c \to \infty$ if the abscissa is rescaled by $c^{-3/4}$ and the ordinate by c^{-1}. (c) The scaling functions ($c = .5, .25, .1, .05, .01, .001$ from top to bottom) asymptotically collapse onto a piecewise linear profile for $c \to 0$ if the abscissa is rescaled by $c^{-1/4}$.

Propagation regime. Here we insert the scaling ansatz $f(s,t) \equiv f_{\rm ext}\varphi(\xi)$ with $\xi = s/\ell_\parallel^*(t)$ and the tentative scaling $\ell_\parallel^*(t) = \ell_{\rm p}^{1/2} f_{\rm ext}^{3/4} t^{1/2}$ as proposed by BBG. This leads to an ordinary differential equation

$$\partial_\xi^2 \varphi = -\frac{1}{8} \xi \varphi^{-3/2} \partial_\xi \varphi. \qquad (25)$$

Boundary conditions are $\varphi(0) = 1$ and $\varphi(\xi \to \infty) = c$ where $c \equiv f_{\rm pre}/f_{\rm ext}$ is the force ratio. This is the same equation as eq. (18) of ref. [16], safe for a factor $\frac{1}{4}$ due to a slightly different definition of the scaling variable ξ. We have solved it numerically by a shooting method. Starting with $\varphi(0) = 1$, it is integrated forward, adjusting the slope $\partial_\xi\varphi(0)$ at the left boundary in order to fulfill the second boundary condition. The dependence of the slope $\partial_\xi\varphi(0)$ on the force ratio c is shown in fig. 4(a), together with the asymptotes for $c \to \infty$ and $c \to 0$, respectively. These shall now be analyzed in more detail.

The case $c > 1$ corresponds to a stretching force $f_{\rm ext} < f_{\rm pre}$ that is decreased at $t = 0$, i.e., a "sudden release"-scenario as in refs. [16, 19, 27]. Since $f_{\rm pre}$ is the relevant force scale, the scaling ansatz is more appropriately written as $f(s,t) = c\, f_{\rm ext}\varphi(c^{-3/4}\xi)$. Now we can safely take the limit $c \to \infty$ ($f_{\rm ext} \to 0$) describing the case where

the force is switched off completely,[3] because the artificial $c^{1/4}$-divergence in $\partial_\xi\varphi(0)$ has been removed. The resulting boundary layer size scales like $\ell_\parallel(t) \simeq \ell_\mathrm{p}^{1/2} f_\mathrm{pre}^{3/4} t^{1/2}$ as in ref. [16] and the corresponding scaling functions, shown in fig. 4(b), smoothly converge to the solutions depicted in refs. [16,27].

The opposite limit $c \to 0$ is more subtle. Although it is not obvious from eq. (25), we may not simply set $f_\mathrm{pre} = 0$ as in ref. [16], since then the condition $f_\mathrm{pre} F \gg 1$ in eq. (21b) cannot be met. Moreover, considering the limit $c \to 0$ with $f_\mathrm{pre} > 0$ fixed instead, our numerical results (fig. 4(a)) indicate that the initial slope $\partial_\xi\varphi(0)$ diverges like $c^{-1/4}$. This suggests the scaling variable $\eta \equiv c^{-1/4}\xi = s/\ell_\parallel(t)$ with the new boundary layer scaling $\ell_\parallel(t) = c^{1/4}\ell_\parallel^*(t) = \ell_\mathrm{p}^{1/2} f_\mathrm{pre}^{1/4} (f_\mathrm{ext} t)^{1/2}$ as anticipated in eq. (13c). We can further rationalize this asymptotic scaling by inserting the improved scaling ansatz $F(s,t) = f_\mathrm{ext} t\, \phi(\eta)$ into eq. (23), which gives $\partial_\eta^2\phi(\eta) = \frac{1}{2} + \mathcal{O}(c^{1/2})$. In the limit $c \to 0$, the scaling function ϕ is parabolic in the boundary region $\eta \in [0,2]$, and the scaling function $\varphi = \phi - \frac{1}{2}\eta\partial_\eta\phi = 1 - \frac{1}{2}\eta$ for the tension f becomes linear. Numerical solutions to eq. (25) in terms of $\eta = \xi c^{-1/4}$ in fact tend towards a piecewise linear function with a kink fixed at $\eta = 2$ (see fig. 4(c)), hence the kink is moving towards vanishing $\xi = c^{1/4}\eta$ as $c \to 0$. This reveals that the limit $c \to 0$ cannot properly be taken in terms of the original scaling variable ξ, because eq. (23) and therefore eq. (25) become invalid if $c = f_\mathrm{pre}/f_\mathrm{ext} = 0$.

Relaxation regime. In the relaxation regime $t \gg t_\star$ we expect the tension to deviate only slighly from the flat equilibrium profile $F \equiv f_\mathrm{ext}\, t$, see fig. 3. We therefore write $F(s,t) = f_\mathrm{ext}\, t + \delta F(s,t)$ and expand eq. (23), which gives the *time-independent* correction:

$$\delta F = \frac{1}{4\ell_\mathrm{p}} \left[f_\mathrm{pre}^{-1/2} - f_\mathrm{ext}^{-1/2} \right] s(s-L). \qquad (26)$$

This result has two significant implications. First of all, in order to estimate the time $t_\star$ beyond which δF becomes small compared to $f_\mathrm{ext}\, t$, we evaluate $\delta F(t_\star) = f_\mathrm{ext}\, t_\star$ and find that not always $t_\star \simeq t_L^\parallel$, see the last two rows of table 1. We find for $f_\mathrm{pre} \gg f_\mathrm{ext}$ and $f_\mathrm{pre} \gg f_\mathrm{c}$ another intermediate regime $t_L^\parallel \ll t \ll t_\star$ of *homogeneous tension relaxation*, where the tension f has a more complicated than just parabolic spatial dependence and the simple ansatz $F(s,t) = f_\mathrm{ext}\, t + \delta F(s,t)$ for the relaxation regimes does not work. This has been attributed [19] to the fact that longitudinal friction may play an essential role also for times $t \gg t_L^\parallel$ beyond the propagation regime and significantly slow down the relaxation. Safe for small correction terms (see appendix A.2), our results for the homogeneous relaxation regime are identical to the "sudden release"-case $f_\mathrm{ext} = 0$ discussed in ref. [27].

[3] If for strongly prestretched "flexible WLC" with $\ell_\mathrm{p} \ll L$ and $f_\mathrm{pre} \gg \ell_\mathrm{p}^{-2}$ the external force is decreased too much ($f_\mathrm{ext} \lesssim \ell_\mathrm{p}^{-2}$), the weakly-bending approximation eventually breaks down near the ends as the tension decreases. This restricts the applicability of our analysis to the dynamics of those observables that are insensitive to boundary contributions [27].

	$t_L^\parallel$	$t_\star$
$f_\mathrm{pre} \ll f_\mathrm{ext} \ll f_\mathrm{c}$	L^8/ℓ_p^4	
$f_\mathrm{ext} \ll f_\mathrm{pre} \ll f_\mathrm{c}$		
$f_\mathrm{pre} \ll f_\mathrm{c} \ll f_\mathrm{ext}$	$L^4/(\ell_\mathrm{p}^2 f_\mathrm{ext})$	
$f_\mathrm{c} \ll f_\mathrm{pre} \ll f_\mathrm{ext}$	$L^2/(\ell_\mathrm{p} f_\mathrm{pre}^{1/2} f_\mathrm{ext})$	
$f_\mathrm{ext} \ll f_\mathrm{c} \ll f_\mathrm{pre}$	$L^2/(\ell_\mathrm{p} f_\mathrm{pre}^{3/2})$	L^8/ℓ_p^4
$f_\mathrm{c} \ll f_\mathrm{ext} \ll f_\mathrm{pre}$		$L^2/(\ell_\mathrm{p} f_\mathrm{ext}^{3/2})$

Table 1. Crossover times $t_L^\parallel$ and $t_\star$ depending on the magnitude of f_pre and f_ext relative to the critical force $f_\mathrm{c} = \ell_\mathrm{p}^2/L^4$.

Secondly, a time-independent correction δF of the integrated tension yields an actual tension $f = \partial_t F$ that (to leading order) does not deviate at all from the flat equilibrium profile $f \equiv f_\mathrm{ext}$. The relaxation dynamics saturates *prematurely* to equilibrium, i.e., at times $t \simeq t_\star$ long before the longest bending mode has relaxed (see also eq. (37) below). This behavior arises within a scenario where a strong stretching force $f_\mathrm{pre} \gg f_\mathrm{c}$ is changed to $f_\mathrm{ext} \gg f_\mathrm{c}$ but remains strong. Hence, there is no need to destroy (create) long-wavelength contributions in the mode spectrum of the stored length (see eq. (6)) as in the "pulling"("release")-scenario of ref. [19]. By taking the next-to-leading order term in the quasi-static approximation [eq. (23)] (cf. appendix A.2), we find an improved correction term that captures the slow diffusive relaxation of the remaining long-wavelength modes:

$$\delta F(s,t) = \frac{1}{4\ell_\mathrm{p}} \left(f_\mathrm{pre}^{-1/2} - f_\mathrm{ext}^{-1/2} \right) s(s-L) - \frac{1}{4\ell_\mathrm{p}} \frac{f_\mathrm{pre}^{-1} - f_\mathrm{ext}^{-1}}{\sqrt{2\pi}(f_\mathrm{ext}\, t)^{1/2}} s(s-L). \qquad (26')$$

Having discussed some of the asymptotic solutions to eq. (10) resulting from the linear, the taut-string, and the quasi-static approximation, respectively, we now present a numerical approach to solve eq. (10).

4 Numerical approach

While the intermediate asymptotes of eq. (10) serve to expose the relevant physics involved in the relaxation process, experiments on the biopolymers we have in mind are usually performed in intermediate, non-asymptotic parameter ranges. Therefore we devised a numerical scheme to solve the nonlinear PIDE [eq. (10)] under very general initial and boundary conditions, allowing eq. (10) to be applied to far more scenarios than just the ones analyzed in this work.

Numerical solutions of eq. (10) are written in terms of dimensionless variables. Here, we use a characteristic

length scale s_c specified when necessary, and the time and force scales $t_f = f_{ext}^{-2}$ and f_{ext}, respectively. The integrated tension is written as

$$F(s,t) \equiv f_{ext}\, t\, \Phi\left(\frac{s}{s_c}, \frac{t}{t_f}\right), \tag{27}$$

and the actual tension profile is then extracted via

$$f(s,t) = f_{ext}\, \varphi(\sigma,\tau) \equiv f_{ext}\, \partial_\tau[\tau\Phi(\sigma,\tau)]. \tag{28}$$

Inserting the scaling form [eq. (27)] into eq. (10) and rescaling $q = \tilde{q}\sqrt{f_{ext}}$ and $t' = zt$, we are left with

$$\Lambda^2\, \partial_\sigma^2\Phi(\sigma,\tau) = \int_0^\infty \frac{\mathrm{d}\tilde{q}}{\pi}\left[\frac{1-\mathrm{e}^{-2\tilde{q}^2\tau[\tilde{q}^2+\Phi(\sigma,\tau)]}}{\tau(\tilde{q}^2+c)} - 2\tilde{q}^2\int_0^1 \mathrm{d}z\, \mathrm{e}^{-2\tilde{q}^2\tau[\tilde{q}^2(1-z)+\Phi(\sigma,\tau)-z\Phi(\sigma,\tau z)]}\right]. \tag{29}$$

The remaining parameters are

$$\Lambda^2 = \ell_p/(f_{ext}^{1/2}s_c^2) \text{ and } c = f_{pre}/f_{ext}. \tag{30}$$

For the "semi-infinite" polymers with $L \to \infty$ we use $\Lambda^2 = 1$ by choosing $s_c = \ell_p^{1/2} f_{ext}^{-1/4}$, while in the finite case the appropriate choice is $s_c = L$.

Our strategy is as follows. Given the initial condition $\varphi(\sigma,0) \equiv \varphi_0(\sigma)$ and appropriate linear boundary conditions for the respective scenario, we introduce a discretized time coordinate τ_n for $n = 0,\dots N$. At each time step τ_n we obtain a two-point boundary value problem:

$$\partial_\sigma^2\Phi(\sigma,\tau_n) = G[\Phi(\sigma,\tau_k)_{k\le n}]. \tag{31a}$$

The nonlinear term G depends also on "earlier" solutions $\Phi(\sigma,\tau_k)$ with $k \le n$. We allow arbitrary linear boundary conditions incorporated via 6 coefficients α_{jk}:

$$\alpha_{00}\Phi(0,\tau_n) + \alpha_{01}\partial_\sigma\Phi(0,\tau_n) = \alpha_{02} \tag{31b}$$

$$\alpha_{10}\Phi(\sigma_M,\tau_n) + \alpha_{11}\partial_\sigma\Phi(\sigma_M,\tau_n) = \alpha_{12}. \tag{31c}$$

These boundary value problems [eq. (31)] are solved by transforming to a system of nonlinear equations using the discretized arclength coordinate σ_m for $m = 0,\dots M$, and discrete representations for the differential operators ∂_σ and ∂_σ^2. For details see Appendix B.

Given numerical solutions to eq. (10), it is straightforward to obtain results for pertinent observables.

5 Results for the change in projected length

The observable of highest interest in experiments is certainly the change in end-to-end distance. Since the sudden change in stretching force (from f_{pre} to f_{ext}) induces the creation or destruction of stored length, and since the total contour length is conserved, we can simply evaluate the change in end-to-end distance (approximated by its projection onto the longitudinal reference axis) by integrating up the total difference in stored length:

$$\begin{aligned}\Delta\overline{R}_\parallel(t) &= -\int_0^L \mathrm{d}s\,[\varrho(s,t)-\varrho(s,0)]\\ &= \int_0^L \mathrm{d}s\,\partial_s^2 F(s,t)\\ &= F'(L,t) - F'(0,t).\end{aligned} \tag{32}$$

Here we have used eq. (8) to relate the change in stored length to the curvature of the integrated tension F. The notation $\Delta\overline{R}_\parallel(t)$ serves as a remainder of the fact that $\Delta\overline{R}_\parallel(t)$ includes only bulk contributions. The "real" change in projected end-to-end distance $\langle \Delta R_\parallel(t)\rangle$ measured in experiments also contains end contributions that depend on the choice of boundary conditions which we have neglected in our approximate mode decomposition of eq. (2). However, a careful analysis [27] shows that for hinged or clamped ends and a sufficiently large prestretching force $f_{pre} \gg L^{-2}$ these contributions vanish. For the "semi-infinite" polymers discussed above we neglected the presence of a second end; here we can exploit the symmetry of the setup and use $\Delta\overline{R}_\parallel(t) = -2F'(0,t)$.

5.1 Analytical results

Given the two forces f_{ext} and f_{pre}, and the additional force scale f_c, the sequence of asymptotic regimes realized for a specific choice of parameters depends on their respective ratios and is in general quite complicated, see also table 1. Relaxing the condition $f_{ext} > f_{pre}$ of sec. 2, we chose to first illustrate schematically the general dependence on the force ratio f_{pre}/f_{ext} since the systematic investigation of its influence is the major novelty of this work. With our numerical results, we will then demonstrate the dependence on the polymer length (more specifically, on the parameter Λ^2 of eq. (30)) for fixed force ratio.

Using eq. (32), we summarized the asymptotic growth laws for $\Delta\overline{R}_\parallel(t)$ resulting from the tension profiles computed in sec. 3 in two phase diagrams. We illustrate the growth laws for $\Delta\overline{R}_\parallel(t)$ as boxed formulas in their respective asymptotic regime depending on the force ratio f_{pre}/f_{ext} in fig. 5 for the propagation regime ($t \ll t_L^\parallel$) and in fig. 6 for the relaxation regime ($t \gg t_\star$), respectively. Given a specific force ratio, the evolution of $\Delta\overline{R}_\parallel(t)$ corresponds to a vertical line through fig. 5 until $t \simeq t_L^\parallel$ where it crosses over to the relaxation regimes ($t \gg t_\star$) depicted in fig. 6, since in most cases $t_L^\parallel \simeq t_\star$.

Let us first turn to the propagation regimes of fig. 5. In the universal initial regime (light shaded) the scaling is linear in the force difference $\Delta f = f_{ext} - f_{pre}$, see eq. (19); it is followed by a quasi-static regime (white) with different force scaling for asymptotically small ($<$) and large ($>$) force ratio; in these limits, we find analytical values for the prefactors $b^>$ and $b^<$ as shown in the figure caption.

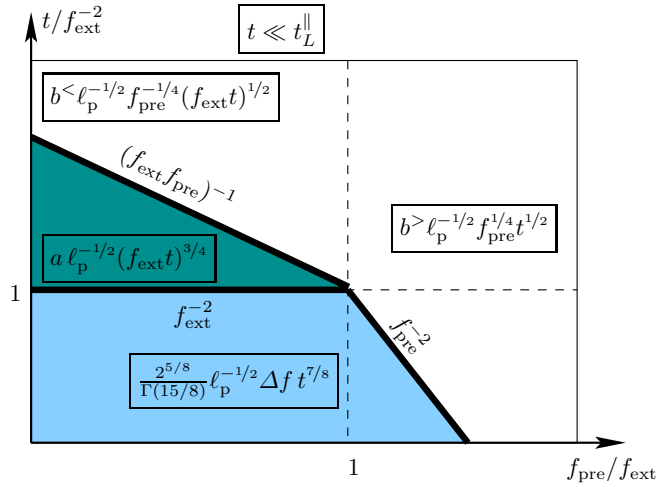

Fig. 5. Regimes of intermediate asymptotics (separated by thick black lines) for the bulk contribution to the change in end-to-end distance $\Delta\overline{R}_{\parallel}(t)$ (boxed formulas) in the propagation regime $t \ll t_L^{\parallel}$; time $t/f_{\rm ext}^{-2}$ vs. force ratio $f_{\rm pre}/f_{\rm ext}$ (log-log scale). Asymptotic values for the prefactors are $b^{<} \sim 2$, $b^{>} \sim -2.48$, and $a = 4(2/\pi)^{1/4}/\sqrt{3}$. See text for explanation.

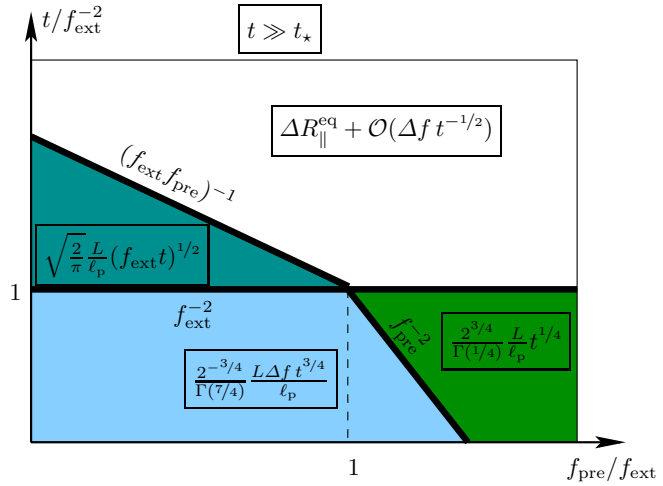

Fig. 6. Regimes of intermediate asymptotics for $\Delta\overline{R}_{\parallel}(t)$ as in fig. 5, but here for the relaxation regime $t \gg t_\star$. See text for explanation.

The general formula follows from eq. (23) and reads

$$\Delta\overline{R}_{\parallel}(t) = -4\partial_\xi\varphi(0)\ell_{\rm p}^{-1/2} f_{\rm ext}^{1/4} t^{1/2}, \tag{33}$$

where the dependence of the slope $\partial_\xi\varphi(0)$ on the force ratio $c = f_{\rm pre}/f_{\rm ext}$ is depicted in fig. 4. The intermediate taut-string region (dark shaded) emerges only for very small force ratio. Here the analytical value for the prefactor a applies to the case $f_{\rm pre} = 0$.

Except for the case $f_{\rm pre} \gg f_{\rm ext}, f_{\rm c}$, the propagation-relaxation crossover at $t \simeq t_L^{\parallel}$ leads directly to the regimes depicted in fig. 6. Here we find again a short-time regime linear in Δf, followed by two different intermediate regimes: the one with small $f_{\rm pre}/f_{\rm ext}$ connects to the "pulling"-case ($f_{\rm pre} = 0$), the other with large force ratio connects to the "release"-case ($f_{\rm ext} = 0$) of ref. [27], respectively. In the final regime $t \gg t_\star$ with $f_{\rm ext}, f_{\rm pre} \gg f_{\rm c}$, the to leading order time-independent correction δF to the equilibrium tension profile [eq. (26)] implies via eq. (32) that $\Delta\overline{R}_{\parallel}(t)$ prematurely attains its equilibrium value

$$\Delta R_{\parallel}^{\rm eq} = \frac{L}{2\ell_{\rm p}} \left[f_{\rm pre}^{-1/2} - f_{\rm ext}^{-1/2} \right]. \tag{34}$$

From eq. (26') we find the subdominant correction term

$$\Delta\overline{R}_{\parallel}(t) = \Delta R_{\parallel}^{\rm eq} - \frac{\Delta f\, L}{\sqrt{32\pi}\ell_{\rm p} f_{\rm pre} f_{\rm ext}^{3/2} t^{1/2}}. \tag{35}$$

The intermediate regime of homogeneous tension relaxation $t_L^{\parallel} \ll t \ll t_\star$ is discussed in ref. [27] and Appendix A.2. For $f_{\rm pre} \gg f_{\rm c}, f_{\rm ext}$ we obtain from eqs. (56b,32) the expansion:

$$\Delta\overline{R}_{\parallel}(t) = -\left(\frac{18Lt}{\ell_{\rm p}^2} \right)^{1/3} + L\,\mathcal{O}\left((t/t_\star)^{2/3} \right). \tag{36}$$

5.2 Numerical results

Using the algorithm outlined in sec. 4, we solved eq. (29) assuming a polymer of finite length L for various values of the two parameters c and Λ^2. The observable $\Delta\overline{R}_{\parallel}(t)$ is then extracted from the slope of the profile at $s = 0$ and $s = L$ via eq. (32). As we analyzed the effect of the *ratio* $f_{\rm pre}/f_{\rm ext}$ of the two force scales present in our scenario in the previous sec. 5.1, we concentrate now on the *magnitude* of the force $f_{\rm ext}$ relative to the critical force $f_{\rm c}$ via the control parameter $\Lambda^2 = \sqrt{f_{\rm c}/f_{\rm ext}}$ for fixed ratio $f_{\rm pre}/f_{\rm ext}$. In fig. 7, we depict results for $f_{\rm pre}/f_{\rm ext} = 10^{-4}$ and various values of Λ^2, i.e., for a sudden increase in stretching force. One can discern the intermediate regime at times $f_{\rm ext}^{-2} \ll t \ll (f_{\rm ext} f_{\rm pre})^{-1}$, which vanishes if the stretching force is changed only slightly. In the limit $f_{\rm pre} = 0$, it connects to the "nonlinear MSPT" propagation ($t \ll t_L^{\parallel}$) and "nonlinear OPT" relaxation ($t \gg t_\star$) regimes of the "pulling"-scenario discussed in ref. [19], respectively. Fig. 8 shows results for the inverse scenario, a sudden decrease in the stretching force, with $f_{\rm pre}/f_{\rm ext} = 10^4$. Here, the time window $f_{\rm pre}^{-2} \ll t \ll f_{\rm ext}^{-2}$ produces a separate asymptotic regime only in the relaxation phase which connects to the regime of nonlinear OPT relaxation [19] of the "release"-scenario if $f_{\rm ext} = 0$. The time window $t_L^{\parallel} \ll t \ll t_\star$ for the regime of homogeneous tension relaxation with its $t^{1/3}$-scaling gets broader as $f_{\rm pre}/f_{\rm ext} \to \infty$.

Because of purely numerical noise in figs. 7 and 8, we have replaced the long-time asymptote of $\Delta\overline{R}_{\parallel}(t)$ for $\Lambda^2 \gg 1$ with dotted straight lines, because the subdominant $\mathcal{O}(t^{-1/2})$-corrections in eq. (35) become smaller than the numerical resolution and it is not possible anymore to reliably evaluate eq. (32). The dashed lines in figs. 7 and 8 indicate the asymptotic growth laws for $\Delta\overline{R}_{\parallel}(t)$ in the

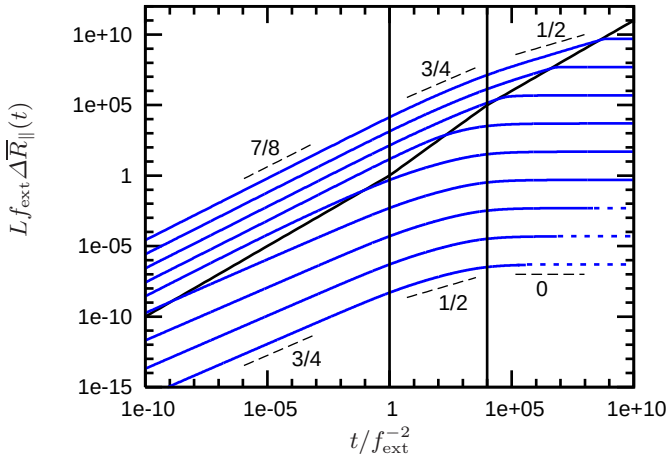

Fig. 7. Numerical results for $\Delta\overline{R}_\parallel(t)$ for $f_{\rm pre}/f_{\rm ext} = 10^{-4}$ and $\Lambda^2 = 10^{-8\ldots8}$ from top to bottom. The dark vertical lines mark the crossovers at $t = f_{\rm ext}^{-2}$ (left) and $t = (f_{\rm ext} f_{\rm pre})^{-1}$ (right), while the dark diagonal line denotes the crossover at $t = t_L^\parallel \simeq t_\star$, see table 1. The dashed lines indicate the asymptotic power laws of figs. 5 and 6.

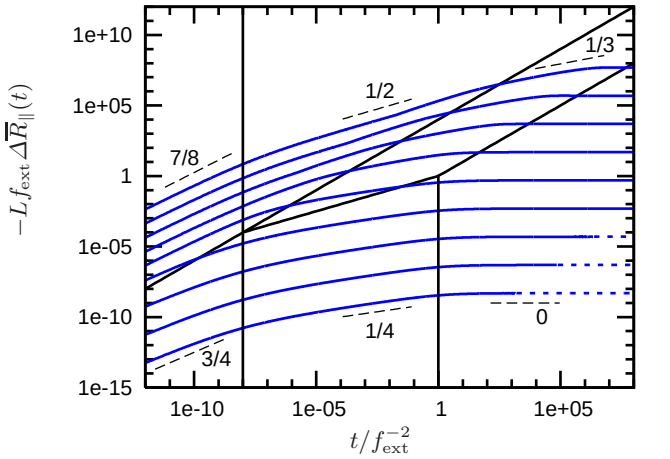

Fig. 8. Numerical results for $\Delta\overline{R}_\parallel(t)$ for $f_{\rm pre}/f_{\rm ext} = 10^4$ and $\Lambda^2 = 10^{-8\ldots8}$ from top to bottom. The dark vertical lines mark the crossover at $t = f_{\rm pre}^{-2}$ (left) and $t = f_{\rm ext}^{-2}$ (right), the dark diagonals mark the crossover at $t = t_L^\parallel$ (upper) and $t = t_\star$ (lower). See table 1. The dashed lines indicate the asymptotic power laws of figs. 5 and 6, and of eq. (36).

respective regimes summarized in figs. 5 and 6. By actually collapsing the corresponding tension profiles onto the scaling functions derived in sec. 3 and appendix A.2, we find excellent quantitative confirmation of our analytical approximations in the suitable asymptotic limits (results not shown).

5.3 Experimental implications

The numerical results for $\Delta\overline{R}_\parallel(t)$ as shown in figs. 7 and 8 over 20 time decades confirm the intermediate asymptotics of eq. (10). They can also be used to fit actual experiments, if one keeps in mind that these unbounded asymptotic growth laws arise from superponing the exponential relaxation of (infinitely) many modes of wavelength $0 < q < \infty$ with relaxation times $\tau_q \simeq q^{-2}/(q^2+f)$, see the response function $\chi_\perp(q;t,t')$ [eq. (4)]. A real polymer provides mode cutoffs at $q_{\rm max} \simeq \pi/a$ where a is some microscopic length scale (say, the polymer thickness) and at $q_{\rm min} \simeq \pi/L$. The latter cutoff defines a time scale $t_L^\perp$, which is the relaxation time of the longest bending mode:

$$t_L^\perp \simeq \begin{cases} L^4, & \text{if } f_{\rm ext} \ll L^{-2}, \\ L^2 f_{\rm ext}^{-1}, & \text{if } f_{\rm ext} \gg L^{-2}. \end{cases} \qquad (37)$$

For times beyond $t_L^\perp$, the continuum limit $L \to \infty$, i.e., disregarding the proper boundary condition and the discreteness of the mode spectrum, becomes invalid; the algebraic relaxation ends and is followed by normal exponential relaxation. Since the crossover times $t_L^\parallel$, $t_\star$, and $t_L^\perp$ depend quite strongly on experimental control parameters such as stretching force, filament length, and persistence length, it is nevertheless possible to cover a broad window of stretching and relaxation dynamics ($t \ll t_L^\perp$) by adjusting these parameters. Our numerical solutions can easily be adapted to the specific experimental setup at hand and provide a quantitative description without free parameters.

6 Conclusions

We have analyzed the generic scenario of a semiflexible filament prestretched with a force $f_{\rm pre}$ that is suddenly changed to $f_{\rm ext}$. Related setups involving only one force scale have been discussed previously [13–16], but with diverse results based on partially contradicting approximations. Extending a systematic theory in terms of backbone tension [19] to include two force scales allows to resolve these discrepancies. Based on this tension formalism (for its detailed formulation see ref. [25]), we derived equations of motion and motivated an intuitive blob-picture in order to estimate growth laws for a central quantity, the boundary layer size or tension propagation length $\ell_\parallel(t)$, which is a measure for how far (or how fast) longitudinal correlations spread along the filament. The scaling laws [eq. (13)] for $\ell_\parallel(t)$ have been confirmed by computing tension profiles as scaling solutions to asymptotic differential equations. We find that, for times beyond the initial linear regime, which is dominated by the relaxation of very stiff bending modes, the prestretching force $f_{\rm pre}$ has a significant influence. If $f_{\rm pre} = 0$, slowly relaxing long-wavelength contributions in the initial conformation resist equilibration and dominate the relaxation process: the taut-string approximation applies. If $f_{\rm pre}$ is finite, these modes are removed from the initial configuration. Hence, the dynamics equilibrates locally, which allows for a quasi-static approximation. Only if $f_{\rm pre} \ll f_{\rm ext}$ is very small, there is a crossover from the former to the latter situation. The limiting single-force cases $f_{\rm ext} = 0$ and $f_{\rm pre} = 0$, respectively, analyzed in detail in ref. [27], were also recovered.

However, the associated limits were found to be highly nontrivial, which is reflected quite subtly in the corresponding equations of motion for the tension. These equations follow systematically from the general eq. (10), while the blob picture provides a more intuitive understanding of the underlying process and the complicated intermediate asymptotics it produces. We presented a numerical algorithm to solve eq. (10) for very general initial and boundary conditions, derived new predictions for experimentally relevant observables and checked them against numerical solutions. Finally, the applicability of our results to experiments was discussed. Our findings for the scenario analyzed in this work should be relevant for the viscoelastic response of more complex structures such as biopolymer networks [2, 5]. Further, we argue that the above established dependence of the relaxation process on the *initial* conditions also generalizes to other force protocols, such as (weakly) time-dependent external forces, transverse forces, elongational flows, or scenarios involving sudden temperature changes.

We gratefully acknowledge financial support via the German Academic Exchange Program (DAAD) (OH), by the Deutsche Forschungsgemeinschaft through grant no. Ha 5163/1 (OH) and SFB 486 (BO, EF), of the German Excellence Initiative via the program "Nanosystems Initiative Munich (NIM)" (BO, EF), and through BayEFG (BO).

A Analytical approach (details)

A.1 Asymptotes of eq. (10)

Following the analysis of ref. [27], we note that the Fourier integrals in eq. (10) are dominated by wavenumbers near a q_m where the exponents are of order 1. Explicitly, we find for given time t and integrated tension F the asymptotes:

$$q_\mathrm{m} \simeq \begin{cases} t^{-1/4}, & \text{if } F^2/t \ll 1 \quad (38a) \\ F^{-1/2}, & \text{if } F^2/t \gg 1 \quad (38b) \end{cases}$$

Observing that $q_\mathrm{m} \simeq \ell_\perp^{-1}$ scales like the inverse of the equilibration length $\ell_\perp$ [eq. (12)], we conclude that the first asymptote comprises free (bending-dominated) relaxation where in the response function [eq. (4)] the tension contribution q^2F is subdominant, whereas the second one corresponds to forced (tension-driven) relaxation with the subdominant bending contribution q^4t.

Secondly, we write eq. (10) as

$$\partial_s^2 F = D - S. \tag{39}$$

The two contributions creating curvature in the tension profile have a direct physical interpretation.

$$D = \int_0^\infty \frac{\mathrm{d}q}{\pi\ell_\mathrm{p}} \frac{1-\mathrm{e}^{-2q^2[q^2t+F(s,t)]}}{q^2+f_\mathrm{pre}}, \tag{40a}$$

is of *deterministic* origin since it expresses the relaxation of initially excited modes for a polymer equilibrated under the force f_pre. The second term

$$S = \int_0^\infty \frac{\mathrm{d}q}{\pi\ell_\mathrm{p}} 2q^2 \int_0^t \mathrm{d}t'\, \mathrm{e}^{-2q^2[q^2(t-t')+F(s,t)-F(s,t')]} \tag{40b}$$

is of *stochastic* origin since it comprises the accumulated influence of thermal excitations from times $t' < t$ mediated with the response function $\chi_\perp$ [eq. (4)]. With the general distinction [eq. (38)] in mind, we first turn our attention to the term D. In the bending-dominated case [eq. (38a)] with $F^2/t \ll 1$, we neglect the tension contribution q^2F in the exponent and obtain

$$D \approx D_1 = \int_0^\infty \frac{\mathrm{d}q}{\pi\ell_\mathrm{p}} \frac{1-\mathrm{e}^{-2q^4t}}{q^2+f_\mathrm{pre}} \qquad \text{if } F^2/t \ll 1, \tag{41}$$

which possesses, depending on the magnitude of f_pre, the two asymptotes

$$D_{1,a} \approx \frac{2^{3/4}t^{1/4}}{\Gamma(1/4)\,\ell_\mathrm{p}} \quad \text{if } f_\mathrm{pre}^2 t \ll 1, \quad F^2/t \ll 1 \tag{42a}$$

$$D_{1,b} \approx \frac{1}{2\ell_\mathrm{p} f_\mathrm{pre}^{1/2}} \quad \text{if } f_\mathrm{pre}^2 t \gg 1, \quad F^2/t \ll 1. \tag{42b}$$

In the tension-driven regime $F^2/t \gg 1$, on the other hand, we get for D by neglecting the bending contribution q^4t

$$D \approx D_2 = \int_0^\infty \frac{\mathrm{d}q}{\pi\ell_\mathrm{p}} \frac{1-\mathrm{e}^{-2q^2F}}{q^2+f_\mathrm{pre}} \qquad \text{if } F^2/t \gg 1, \tag{43}$$

which can be expanded for asymptotically small or large ratios of the product Ff_pre. The leading-order terms are

$$D_{2,a} \approx \sqrt{\frac{2F}{\pi\ell_\mathrm{p}^2}} \qquad \text{if } Ff_\mathrm{pre} \ll 1, \quad F^2/t \gg 1 \tag{44a}$$

$$D_{2,b} \approx \frac{1}{2\ell_\mathrm{p} f_\mathrm{pre}^{1/2}} \quad \text{if } Ff_\mathrm{pre} \gg 1, \quad F^2/t \gg 1. \tag{44b}$$

The stochastic term S is simpler. In the regime $F^2/t \ll 1$ we neglect the tension terms and simplify

$$\begin{aligned} S \approx S_1 &= \int_0^\infty \frac{\mathrm{d}q}{\pi\ell_\mathrm{p}} 2q^2 \int_0^t \mathrm{d}t'\, \mathrm{e}^{-2q^4(t-t')} \\ &= \int_0^\infty \frac{\mathrm{d}q}{\pi\ell_\mathrm{p}} \frac{1-\mathrm{e}^{-2q^4t}}{q^2} \\ &= \frac{2^{3/4}t^{1/4}}{\Gamma(1/4)\,\ell_\mathrm{p}}, \qquad \text{if } F^2/t \ll 1. \end{aligned} \tag{45}$$

For $F^2/t \gg 1$, the t'-integral in the stochastic term S is dominated by contributions near the upper limit and we can linearize $F(s,t) - F(s,t') \approx \partial_t F(s,t)(t-t')$:

$$\begin{aligned} S \approx S_2 &= \int_0^\infty \frac{\mathrm{d}q}{\pi\ell_\mathrm{p}} 2q^2 \int_0^t \mathrm{d}t'\, \mathrm{e}^{-2q^2(t-t')[q^2+\partial_t F]} \\ &= \int_0^\infty \frac{\mathrm{d}q}{\pi\ell_\mathrm{p}} \frac{1-\mathrm{e}^{-2q^2t[q^2+\partial_t F]}}{q^2+\partial_t F} \\ &\approx \int_0^\infty \frac{\mathrm{d}q}{\pi\ell_\mathrm{p}} \frac{1}{q^2+\partial_t F} \\ &= \frac{1}{2\ell_\mathrm{p}\sqrt{\partial_t F}}, \qquad \text{if } F^2/t \gg 1. \end{aligned} \tag{46}$$

In the third line we neglected the exponential in the limit $F^2/t \gg 1$, which expresses the instantaneous equilibration underlying the quasi-static approximation of ref. [16]; this is an expansion similar to the one leading to eq. (44b).

A.2 Aymptotic equations of motion and solutions for the relaxation regime

The asymptotic forms of eq. (10) used in sec. 3 were motivated physically and based on approximations employed previously [13, 15, 16], but can also systematically be derived. The right hand side $D-S$ of eq. (39) was analyzed in app. A.1 for asymptotes of the deterministic and stochastic term D and S, respectively, see eqs. (42,44,45,46). Now we can treat these various limits separately and find solutions for the relaxation regimes omitted in sec. 3. For $t \gg t_\star$ we can exploit the fact that in this time regime the tension deviates only by a small correction δF from the flat equilibrium profile $f_{\rm ext}t$. It is therefore possible to expand the right hand side of eq. (10) about this constant, which to lowest order gives $\partial_s^2 \delta F \approx [D-S]_{F\to f_{\rm ext}t}$.

1. If $F^2/t \ll 1$ and $f_{\rm pre}^2 t \ll 1$, we obtain $D \approx D_{1,a}$ and $S \approx S_1$, which cancel to leading order. But since the preconditions imply small F and $f_{\rm pre}$, the right-hand-side of eq. (39) can be linearized with respect to these quantities. This was performed in sec. 3.1, see eq. (14), and lead via a Laplace transform to the tension profile eq. (17). In the relaxation regime $L \ll \lambda$ with $\lambda(z) = 2^{3/8}\ell_{\rm p}^{1/2} z^{-1/8}$, we obtain the following tension profile:
$$\tilde{F}(s,z) = \frac{f_{\rm ext}}{z^2} + \frac{\Delta f}{z^2}\frac{s(s-L)}{2\lambda^2}. \tag{47}$$
Backtransforming, we get
$$F(s,t) = f_{\rm ext}t + \frac{\Delta f\, t^{3/4}}{2^{7/4}\Gamma(7/4)\,\ell_{\rm p}} s(s-L), \tag{48}$$
i.e., a small correction δF to the equilibrium tension $f_{\rm ext}t$ if $t \gg t_\star = L^8/\ell_{\rm p}^4$.
2. $F^2/t \ll 1$ and $f_{\rm pre}^2 t \gg 1$ gives $D \approx D_{1,b}$ and $S \approx S_1$, hence
$$\partial_s^2 F = D_{1,b} - S_1 \approx -S_1. \tag{49}$$
This implies constant curvature (no propagation) in the time regime $f_{\rm pre}^{-2} \ll t \ll f_{\rm ext}^{-2}$. The tension reads
$$F(s,t) = f_{\rm ext}t + \frac{2^{-1/4}t^{1/4}s(s-L)}{\Gamma(1/4)\,\ell_{\rm p}}. \tag{50}$$
3. $F^2/t \gg 1$ and $F f_{\rm pre} \ll 1$ yields
$$\partial_s^2 F \approx D_{2,a} - S_2 \approx D_{2,a}, \tag{51}$$
which comprises the taut-string case [eq. (21a)]. We discussed the propagation regime in sec. (3.2); the relaxation regime follows by writing $F(s,t) = f_{\rm ext}t + \delta F(s,t)$ and expanding, which yields
$$\delta F(s,t) = \frac{(f_{\rm ext}t)^{1/2}}{\sqrt{8\pi}\ell_{\rm p}} s(s-L). \tag{52}$$
4. $F^2/t \gg 1$ and $F f_{\rm pre} \gg 1$ leads to
$$\partial_s^2 F \approx D_{2,b} - S_2, \tag{53}$$
which corresponds to the quasi-static approximation [eq. (23)]. We discussed the propagation regime $t \ll t_L^{\parallel}$ and the regime of premature tension saturation $t \gg t_\star$ in sec. 3.3. In the latter case, we used for eq. (26') the next-to-leading order terms of the asymptotic expansions eqs. (44b,46). For $f_{\rm pre} \gg f_{\rm ext}$ and $f_{\rm pre} \gg f_{\rm c}$ remains an intermediate regime $t_L^{\parallel} \ll t \ll t_\star$ of homogeneous tension relaxation, see table 1. It turns out to be very related to the "release"-case $f_{\rm ext} = 0$ of ref. [27]. It is not possible to expand $F(s,t) = f_{\rm ext}\,t + \delta F$, since the correction δF is for $t \ll t_\star$ not (yet) small compared to $f_{\rm ext}\,t$. However, as in ref. [27] for $f_{\rm ext} = 0$, we can solve eq. (24) using the separation ansatz $f(s,t) = g(t)h(s/L)$ and compute correction terms in the limit $f_{\rm pre} \gg f_{\rm ext}$. Disregarding the proper initial conditions and assuming Dirichlet boundary conditions for the moment, we find that asymptotically
$$g(t) \sim \left(\frac{L^2}{\ell_{\rm p}t}\right)^{2/3}. \tag{54}$$
Although this is a decreasing function of time, we find that if $t \ll L^8/\ell_{\rm p}^4$ the preconditions ($f^2 t \gg 1$ and $F f_{\rm pre} \gg 1$) that lead to the asymptotic eq. (24) are fulfilled. In order to correct the Dirichlet boundary conditions assumed above to $h(0) = h(1) = \gamma(t) \equiv f_{\rm ext}/g(t)$, we require that $t \ll L^2/(\ell_{\rm p} f_{\rm ext}^{3/2})$ which makes $\gamma \ll 1$. Both conditions reduce to $t \ll t_\star$, cf. table 1. The roughly parabolic profile $h(\sigma)$ is a solution of
$$h'' = -\frac{1}{6h^{1/2}}, \quad \text{with } h(0) = h(1) = \gamma(t), \tag{55}$$
where a subdominant time-dependence stems from the small correction term $\gamma(t)$ to the Dirichlet boundary conditions. It has the following characteristics:
$$h(1/2) = \frac{1}{16}\left(\frac{3}{2}\right)^{2/3} + \frac{1}{2}\gamma + \mathcal{O}(\gamma^{3/2}), \tag{56a}$$
$$h'(0) = 12^{-1/3} - \left(\tfrac{2}{3}\right)^{2/3}\gamma^{1/2} + \mathcal{O}(\gamma^{3/2}). \tag{56b}$$

B Numerical approach (details)

B.1 Evaluation of the nonlinear term

The computation of the nonlinear term G with its dependence on $\Phi(\sigma,\tau_k)$ requires to evaluate the z-integral in eq. (29). This can be done *analytically*, if a piecewise linear interpolation is used in the exponent:
$$\Phi(\sigma,\tau_n) - z\Phi(\sigma,z\tau_n) \approx A_k + B_k(z_{k+1} - z), \tag{57}$$
for an index $k \in [0, n-1]$ such that $\tau_k \le \tau_n z \le \tau_{k+1}$ and with $z_k = \tau_k/\tau_n$. The linearization coefficients are
$$\begin{aligned} A_k &= \Phi(\sigma,\tau_n) - z_{k+1}\Phi(\sigma,\tau_{k+1}) \\ B_k &= \Phi(\sigma,\tau_{k+1}) + z_{k+1}\frac{\Phi(\sigma,\tau_{k+1}) - \Phi(\sigma,\tau_k)}{z_{k+1} - z_k}. \end{aligned} \tag{58}$$

With the linearization (57), $G[\Phi(\sigma,\tau_n)]$ is expressed as:

$$G[\Phi(\sigma,\tau_n)] = \int_0^\infty \frac{\mathrm{d}\tilde{q}}{\pi}\left[\frac{1-\mathrm{e}^{-2\tilde{q}^2\tau_n[\tilde{q}^2+\Phi(\sigma,\tau_n)]}}{\tau_n(\tilde{q}^2+c)}\right] + \sum_{k=0}^{n-1}\int_0^\infty \frac{\mathrm{d}\tilde{q}}{\pi}\left[\mathrm{e}^{-2\tilde{q}^2\tau_n[\tilde{q}^2(1-z_{k+1})+A_k]} \times \frac{\mathrm{e}^{-2\tilde{q}^2\tau_n(z_{k+1}-z_k)[\tilde{q}^2+B_k]}-1}{\tau_n(\tilde{q}^2+B_k)}\right]. \quad (59)$$

It turns out that the nonlinear problems [eq. (31)] are ill-conditioned in many cases. Their solutions are strongly affected by numerical errors and often the algorithms used to solve these problems fail to converge. Hence, it is necessary to evaluate the nonlinear term [eq. (59)] as accurately as possible. In order to represent the intermediate asymptotic regimes, the variables τ and Φ have to vary over many orders of magnitude. Thus, in eq. (59), we have to take care of overflow/underflow artefacts from the exponential functions. For the numerical evaluation of the $\tilde{q}$-integrals, we need to make sure that the dominant contribution from modes near $q_\mathrm{m} = \tilde{q}_\mathrm{m}\sqrt{f_\mathrm{ext}}$ is properly taken into account; see eq. (38).

B.2 Nonlinear boundary value problems

When solving a two-point boundary value problem with general mixed linear boundary conditions such as eq. (31) (where we omit the dependence on τ_n), the problem is mapped to a system of nonlinear equations. Writing the values $\Phi(\sigma_m) \equiv \Phi_m$, where $m = 0,\ldots,M$, as vector $\boldsymbol{\Phi} = (\Phi_0,\ldots,\Phi_M)^T$, the problem can be posed as

$$\boldsymbol{T}(\boldsymbol{\Phi}) = 0. \quad (60)$$

The nonlinear operator $\boldsymbol{T}$ is defined via the *residuals* of eq. (31):

$$\begin{aligned}(\boldsymbol{T}(\boldsymbol{\Phi}))_m &= \Delta_m\boldsymbol{\Phi} - G[\Phi_m], \qquad m = 1,\ldots,M-1\\ (\boldsymbol{T}(\boldsymbol{\Phi}))_0 &= \alpha_{00}\Phi_0 + \alpha_{01}D_0^+\boldsymbol{\Phi} - \alpha_{02}\\ (\boldsymbol{T}(\boldsymbol{\Phi}))_M &= \alpha_{10}\Phi_M + \alpha_{11}D_M^-\boldsymbol{\Phi} - \alpha_{12}\end{aligned} \quad (61)$$

Here, we have used discrete representations of the differential operators ∂_σ and ∂_σ^2. For the possibly non-uniformly discretized coordinate σ_m with local stepsize $h_m^+ = \sigma_{m+1} - \sigma_m$ and $h_m^- = \sigma_m - \sigma_{m-1}$, they are given by:

$$\begin{aligned}\Delta_m\boldsymbol{\Phi} &= \frac{2}{h_m^-(h_m^-+h_m^+)}\Phi_{m-1} - \frac{2}{h_m^-h_m^+}\Phi_m + \frac{2}{h_m^+(h_m^-+h_m^+)}\Phi_{m+1}\\ D_0^+\boldsymbol{\Phi} &= \frac{1}{h_0^+}(\Phi_1-\Phi_0)\\ D_M^-\boldsymbol{\Phi} &= \frac{1}{h_M^-}(\Phi_M-\Phi_{M-1})\end{aligned} \quad (62)$$

In the formulation [eq. (60)] our task is to find the zero of $\boldsymbol{T}$ in the vector space of discrete function representations $\boldsymbol{\Phi}$. The common strategies are all based on Newton's method [28]. Given an initial guess $\boldsymbol{\Phi}_0$, this iterative method seeks a correction $\boldsymbol{d}$ such that $\boldsymbol{\Phi}_0 + \boldsymbol{d}$ is the solution. If the initial guess is good, the correction is small and we can write

$$\boldsymbol{T}(\boldsymbol{\Phi}_0 + \boldsymbol{d}) \approx \boldsymbol{T}(\boldsymbol{\Phi}_0) + J(\boldsymbol{\Phi}_0)\boldsymbol{d} = 0 \quad (63)$$

with the Jacobian matrix

$$J_{ij}(\boldsymbol{\Phi}) = \frac{\partial \boldsymbol{T}(\boldsymbol{\Phi})_i}{\partial \boldsymbol{\Phi}_j}. \quad (64)$$

This matrix can be computed either analytically or by finite-difference approximation. In principle, the linear equation [eq. (63)] can be solved straightforwardly for the optimal correction $\boldsymbol{d}$:

$$\boldsymbol{d} = -J^{-1}(\boldsymbol{\Phi}_0)\boldsymbol{T}(\boldsymbol{\Phi}_0). \quad (65)$$

Finally, by iterating

$$\boldsymbol{\Phi}_{k+1} = \boldsymbol{\Phi}_k - J^{-1}(\boldsymbol{\Phi}_k)\boldsymbol{T}(\boldsymbol{\Phi}_k), \quad (66)$$

one should finally find the solution $\boldsymbol{\Phi}^\star = \lim_{k\to\infty}\boldsymbol{\Phi}_k$ with $\boldsymbol{T}(\boldsymbol{\Phi}^\star) = 0$. For "well-behaved" operators $\boldsymbol{T}$, this iteration converges quadratically in the vicinity of the solution. Unfortunately, in our case $\boldsymbol{T}$ is often ill-conditioned near the solution. More sophisticated methods therefore modify the iteration [eq. (66)] [28]. Still, a very accurate evaluation of the nonlinear term $G[\Phi]$ in eq. (61) is crucial to ensure convergence. For our implementation, two different algorithms in the GNU scientific library[4] and in the NLEQ package[5] have been used.

B.3 Error control

We can control discretization errors stemming from representing the continuous problem [eq. (29)] as system of nonlinear equations [eq. (60)] by reliable error estimates.

An estimate for the spatial discretization error can be obtained via a deferred corrections approach [31]. The nonlinear system [eq. (60)] is written with the low-order accurate representation [eq. (62)] for the spatial derivatives. Given its low-order accurate solution $\boldsymbol{\Phi}$ and another, high-order accurate operator $\boldsymbol{T}^*$, we can solve the perturbed system $\boldsymbol{T}(\boldsymbol{\Phi}^*) = -\boldsymbol{T}^*(\boldsymbol{\Phi})$ to obtain a high-order accurate solution $\boldsymbol{\Phi}^*$. The discretization error of $\boldsymbol{\Phi}$ is estimated by the difference $\boldsymbol{\Phi}^* - \boldsymbol{\Phi}$. The important point is that not the (possibly complicated) high-order system associated with $\boldsymbol{T}^*$, but only the perturbed low-order system needs to be solved. A high-order accurate operator $\boldsymbol{T}^*$ is obtained by using more accurate representations of the

[4] The GSL is available from `www.gnu.org/software/gsl` and uses Powell's hybrid algorithm [29].

[5] The NLEQ package is available from `www.zib.de` and documented in ref. [30].

derivatives than those in eq. (62), in our case by means of Noumerov's method. Altogether, we obtain at least three digits of accuracy for our choice of discretization. We use "graded" grids, $\sigma_m = \sigma_M (m/M)^\beta$ for $m = 0, \ldots, M-1$. For the semiinfinite polymers, we take $\beta = 1.25$ and dynamically adpat σ_M; otherwise we take $\beta = 1$ and $\sigma_M = 1$.

The discretization error stemming from the τ-discretization needs to be estimated because we want to cover many orders of magnitude in the time variable. Our results show that an exponential growth in τ_n does not increase the discretization error (this is due to the right hand side of eq. (10) becoming asymptotically independent of shorttime effects in the nonlinear regime, cf. eq. (46)). Hence, we choose $\tau_n = \Delta(\delta^n - 1)/(\delta - 1)$ for $n = 0, \ldots, N$ with the initial stepsize Δ and the growth factor $\delta > 1$. To estimate the discretization error, we take "fine" steps $\tilde{\tau}_n = \tau_0(\delta^{n/2} - 1)/(\delta - 1)$ with $n = 0, \ldots, 2N$ such that $\tilde{\tau}_{2n} = \tau_n$. In the step n two additional "fine" solutions $\tilde{\Phi}(\sigma, \tilde{\tau}_{2n-1})$ and $\tilde{\Phi}(\sigma, \tilde{\tau}_{2n})$ are computed. The error estimate follows from the difference $\tilde{\Phi}(\sigma, \tilde{\tau}_{2n}) - \Phi(\sigma, \tau_n)$. Altogether, we get at least three digits of accuracy for our choice of the crucial parameter δ: for the semiinfinite polymers, we take $\delta = 1.1$ (only tension propagation), otherwise $\delta = 1.05$ (also tension relaxation).

References

1. A. R. Bausch and K. Kroy, Nat. Phys. **2**, 231 (2006).
2. M. L. Gardel *et al.*, Proc. Natl. Acad. Sci. USA **103**, 1762 (2006).
3. R. Granek, J. Phys. I (Paris) **7**, 1761 (1997).
4. N. Rosenblatt *et al.*, Phys. Rev. Lett. **97**, 168101 (2006).
5. D. Mizuno, C. Tardin, C. F. Schmidt, and F. C. MacKintosh, Science **315**, 370 (2007).
6. C. Bustamante, Z. Bryant, and S. B. Smith, Nature **421**, 423 (2003).
7. J.-C. Meiners and S. R. Quake, Phys. Rev. Lett. **84**, 5014 (2000).
8. D. Lumma, S. Keller, T. Vilgis, and J. O. Rädler, Phys. Rev. Lett. **90**, 218301 (2003).
9. R. E. Goldstein and S. A. Langer, Phys. Rev. Lett. **75**, 1094 (1995).
10. N.-K. Lee and D. Thirumalai, Biophys. J. **86**, 2641 (2004).
11. Y. Bohbot-Raviv *et al.*, Phys. Rev. Lett. **92**, 098101 (2004).
12. T. B. Liverpool, Phys. Rev. E **72**, 021805 (2005).
13. U. Seifert, W. Wintz, and P. Nelson, Phys. Rev. Lett. **77**, 5389 (1996).
14. A. Ajdari, F. Jülicher, and A. Maggs, J. Phys. I (Paris) **7**, 823 (1997).
15. R. Everaers, F. Jülicher, A. Ajdari, and A. C. Maggs, Phys. Rev. Lett. **82**, 3717 (1999).
16. F. Brochard-Wyart, A. Buguin, and P. G. de Gennes, Europhys. Lett. **47**, 171 (1999).
17. S. Manneville *et al.*, Europhys. Lett. **36**, 413 (1996).
18. B. Maier, U. Seifert, and J. O. Rädler, Europhys. Lett. **60**, 622 (2002).
19. O. Hallatschek, E. Frey, and K. Kroy, Phys. Rev. Lett. **94**, 077804 (2005).
20. P. G. de Gennes, P. Pincus, R. M. Velasco, and F. Brochard, J. Phys. (Paris) **37**, 1461 (1976).
21. N. Saitô, K. Takahashi, and Y. Yunoki, J. Phys. Soc. Jap. **22**, 219 (1967).
22. P. A. Wiggins *et al.*, Nat. Nanotechnol. **1**, 137 (2006).
23. A. K. Mazur, Phys. Rev. Lett. **98**, 218102 (2007).
24. J. Kierfeld, O. Niamploy, V. Sa-yakanit, and R. Lipowsky, Eur. Phys. J. E **14**, 17 (2004).
25. O. Hallatschek, E. Frey, and K. Kroy, Phys. Rev. E **75**, 031905 (2007).
26. F. C. MacKintosh, J. Käs, and P. A. Janmey, Phys. Rev. Lett. **75**, 4425 (1995).
27. O. Hallatschek, E. Frey, and K. Kroy, Phys. Rev. E **75**, 031906 (2007).
28. J. E. Dennis and R. B. Schnabel, *Numerical Methods for Unconstrained Optimization and Nonlinear Equations* (Prentice-Hall, Englewood Cliffs, 1983).
29. M. J. D. Powell, in *Numerical Methods for Nonlinear Algebraic Equations*, edited by P. Rabinowitz (Gordon and Breach, London, 1970), Chap. 6, p. 87.
30. U. Nowak and L. Weimann, Technical Report No. TR-91-10, Konrad-Zuse-Zentrum für Informationstechnik, Berlin (1991).
31. V. Pereyra, Numer. Math. **8**, 376 (1966).